tration. As the sodium concentration increases, the minimum distance, q_{min}, between the Fermi surface and the zone boundary decreases. The contribution of U processes to the lattice Seebeck coefficient will, therefore, increase with increasing sodium concentration. Thus, the lattice Seebeck coefficient should show an increase in the positive phonon-drag contribution with increasing sodium concentration. This behavior is seen in the lattice Seebeck coefficient of Na_xWO_3 (see Fig. 5). For low sodium concentrations there is only a negative contribution to the lattice Seebeck coefficient. However, as the sodium concentration increases, the positive phonon-drag contribution also increases.

We conclude that the Fermi surface of Na_xWO_3 is more complicated than the free-electron sphere, but that the x dependence of the lattice Seebeck coefficient can be qualitatively understood if we assume that the Fermi level increases with increasing number of free electrons.

ACKNOWLEDGMENTS

We wish to thank Dr. R. Fuchs and Dr. A. L. Trego for their helpful discussions. Thanks are also due to O. M. Sevde for his technical assistance, and Miss J. E. Brown for her help in preparing the Na_xWO_3 single crystals.

PHYSICAL REVIEW VOLUME 160, NUMBER 3 15 AUGUST 1967

Electron Energy Levels in Cu_3Au†*

D. GRAY‡ AND E. BROWN
Rensselaer Polytechnic Institute, Troy, New York
(Received 30 January 1967)

Electron energy levels in perfectly ordered Cu_3Au have been calculated using the modified-plane-wave (MPW) method for the majority of points in the Brillouin zone and using the orthogonalized-plane-wave (OPW) method for some of the lower symmetry points. The calculation has been done for the equivalent of 512 points in the reciprocal-space lattice. A muffin-tin model potential has been used. This was constructed from the atomic potentials of Herman and Skillman who did a self-consistent calculation based on the Slater version of the Hartree-Fock equations. This version includes an averaged exchange term. $E(\mathbf{k})$ curves are shown. The Fermi level has been computed to be -0.39 Ry. The resulting Fermi surface compares very well with the simplified surface constructed by Harrison by folding the copper Fermi surface in accord with the new lattice. Calculations were also carried out at a limited number of points for copper using both the Herman-Skillman and the Chodorow potentials in order to examine the sensitivity of the results to difference in potential. The two compare within about 0.04 Ry near the Fermi level but some d-like points differ by as much as 0.1 Ry.

CRYSTAL STRUCTURE AND POTENTIAL

IN the present paper, the band structure of perfectly ordered Cu_3Au is calculated using the modified-plane-wave (MPW) method[1] in conjunction with the orthogonalized-plane-wave (OPW) method. The MPW method was used in order to guarantee convergence from above. However, the OPW method was found to be entirely satisfactory when used with accurate core states. The simple-cubic unit cell for Cu_3Au is shown in Fig. 1. There is one gold atom and three copper atoms associated with each lattice point. In this paper the origin is taken at a gold atom, $\boldsymbol{\tau}$ vectors describe the positions of unit cells, and $\mathbf{s}_\nu$ vectors describe the positions of the basis atoms within a unit cell. As the unit cell is simple cubic, the Brillouin zone is also simple cubic. This is shown in Fig. 2 with the points of high symmetry labeled in the Bouckaert, Smoluchowski, and Wigner (BSW) notation.[2]

The one-electron approach is used. The crystal potential is constructed from the atomic potentials of Herman and Skillman[3] (HS) using the muffin-tin model. In this model we surround the individual atoms with nonoverlapping spheres whose radii are chosen so that the potentials match at the point of contact. Inside each of these spheres we take the crystal potential to be the potential of that particular atom as a free ion and outside the spheres we take the potential to be a constant. The HS potentials were modified slightly so that the Au and Cu potentials join smoothly along a line from Au center to Cu center. The value of the potential at the joining point was used for $\bar{V}$, the constant potential in the region between spheres.

† This paper is a condensed version of a doctoral thesis submitted to Rensselaer Polytechnic Institute in August, 1966 by one of the authors (D.G.).

* This work was supported by the U. S. Atomic Energy Commission.

‡ Now at Watervliet Arsenal, Watervliet, New York.

[1] E. Brown and J. A. Krumhansl, Phys. Rev. **109**, 30 (1958).

[2] L. P. Bouckaert, R. Smoluchowski, and E. Wigner, Phys. Rev. **50**, 58 (1936).

[3] F. Herman and S. Skillman, *Atomic Structure Calculations* (Prentice-Hall, Inc., Englewood Cliffs, New Jersey, 1963).

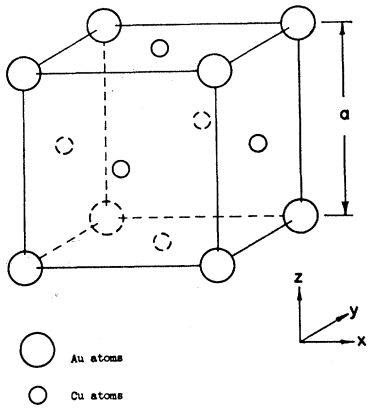

FIG. 1. Unit cell in real space for Cu_3Au.

THE MODIFIED-PLANE-WAVE METHOD

We approximate the true electron wave function $\psi_t^n(\mathbf{r})$ by

$$\psi_a^n(\mathbf{r})=\sum_i C_{ni}\phi_i(\mathbf{r}), \tag{1}$$

where the ϕ_i are known functions and the C_{ni} are determined by the variational procedure. In the MPW method the expansion functions ϕ_i are of two types: (1) plane waves which extend throughout the entire crystal and (2) atomic functions which are zero outside the muffin-tin spheres. The atomic functions are added in order to get high wave-number components into the expansion without using an exorbitantly large number of plane waves. The variational procedure leads to the set of equations

$$\sum_j C_{nj}\int \phi_i^*(\mathbf{r})(\mathbf{H}-E_n)\phi_j(\mathbf{r})d\tau=0, \tag{2}$$

where $\mathbf{H}$ is the Hamiltonian of the system and E_n is the nth energy eigenvalue. (We arbitrarily order the E's from lowest to highest.) These equations are to be solved for each reciprocal-space $\mathbf{k}$ value used. This set is equivalent to the matrix equation

$$\mathbf{H}\mathbf{C}_n=E_n\mathbf{S}\mathbf{C}_n, \tag{3}$$

where

$$H_{ij}=\int \phi_i^*(\mathbf{r})\mathbf{H}\phi_j(\mathbf{r})d\tau, \tag{4}$$

and

$$S_{ij}=\int \phi_i^*(\mathbf{r})\phi_j(\mathbf{r})d\tau. \tag{4'}$$

As the ϕ_i are not necessarily orthogonal, $\mathbf{S}$ is not the identity matrix. However, Eq. (3) is equivalent to the standard eigenvalue equation

$$\mathbf{H}'\mathbf{C}_n'=E_n\mathbf{C}_n', \tag{5}$$

where $\mathbf{H}'$ is the Hermitian matrix $\mathbf{S}^{-1/2}\mathbf{H}\mathbf{S}^{-1/2}$ and $\mathbf{C}_n'=\mathbf{S}^{1/2}\mathbf{C}_n$.

The atomic functions are Bloch sums of atomic orbitals, namely $\sum_j \exp[i\mathbf{k}\cdot(\boldsymbol{\tau}_j+\mathbf{s}_\nu)]F_{nlm}(\mathbf{r}-\boldsymbol{\tau}_j-\mathbf{s}_\nu)$, where F_{nlm} is an atomic orbital. These atomic orbitals are free-atom solutions of the Schrödinger equation with the modification that they are zero outside the atomic spheres. These functions were calculated in a separate program[4] by solving the Schrödinger equation numerically using the appropriate HS potential for each atom. The plane-wave terms are of the form $e^{i(\mathbf{k}+\mathbf{K})\cdot\mathbf{r}}$ where $\mathbf{K}$ is a reciprocal lattice vector. For each symmetry point group theory is used to reduce the number of expansion functions for each representation.

$E(\mathbf{k})$ has been evaluated for the equivalent of 512 uniformly spaced points in $\mathbf{k}$ space. Because of the high degree of symmetry involved it is sufficient to take 35 points in the portion of $\mathbf{k}$ space bounded by $\Gamma\Delta X$, $\Gamma\Lambda R$, $\Gamma\Sigma M$, XZM, XSR, and MTR as indicated in Fig. 2. Summing up all the irreducible representations having levels in the range of interest (roughly -1 Ry to zero) gives a total of 135 separate problems. For some 40 of these problems, the OPW method was used because of the large number of atomic functions involved. In addition there are 12 points of very low symmetry (two members in the group of $\mathbf{k}$) and one general point. These 13 points were calculated by interpolation between neighboring points of higher symmetry.

CALCULATION OF MATRIX ELEMENTS AND DIAGONALIZATION

In calculating the S_{ij} and H_{ij} matrix elements, it is sufficient to symmetrize just one of the ϕ_i, ϕ_j functions. A symmetrized plane wave has the form $\sum_R D_{11}(\mathbf{R})\exp[i(\mathbf{k}+\mathbf{K})\cdot\mathbf{R}\mathbf{r}]$ where the $\mathbf{R}$ are members of the "group of $\mathbf{k}$," a subgroup of the full 48-member cubic group. The $\mathbf{R}$ of this subgroup must satisfy either $\mathbf{R}\mathbf{k}=\mathbf{k}$ or $\mathbf{R}\mathbf{k}=\mathbf{k}+\mathbf{K}$. $D_{11}(\mathbf{R})$ is the "one-one" element of the matrix representing the operator $\mathbf{R}$. A symmetrized atomic function has the form

$$\sum_R D_{11}(\mathbf{R})\sum_j \exp[i\mathbf{k}\cdot(\boldsymbol{\tau}_j+\mathbf{s}_\nu)]F_{nlm}(\mathbf{R}\mathbf{r}-\boldsymbol{\tau}_j-\mathbf{s}_\nu).$$

The matrix elements will be of three types: plane-wave–plane-wave, plane-wave–atomic, and atomic-atomic. The final expressions for these elements are given in an Appendix. The group-theory part of the atomic-atomic terms was calculated by hand. The rest of the operations involved in numerically evaluating the S_{ij}, H_{ij} elements were done on a CDC 6600 computer. Once the S_{ij}, H_{ij} elements have been evaluated a unitary matrix is applied which diagonalizes $\mathbf{S}$ of Eq. (3). We then transform Eq. (3) to the form of Eq. (5) and diagonalize $\mathbf{H}'$ giving the energy eigenvalues. The Jacobi routine was used to carry out the diagonaliza-

[4] We are indebted to Dr. F. K. Bloom for this program.

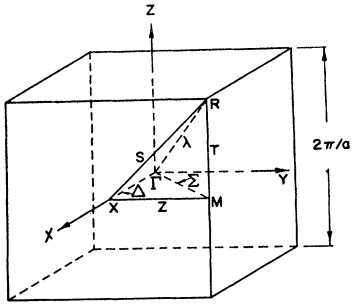

FIG. 2. Unit cell in reciprocal space for Cu_3Au. The symmetry points and axes are labeled in the BSW notation.

tions. The eigenfunctions are also generated by the program.[5]

SENSITIVITY OF ENERGY LEVELS TO THE POTENTIAL CHOSEN

We have also calculated energy levels for a few symmetry points of copper using the HS potential and compared them with the calculation of Burdick.[6] In his band-structure calculation for copper Burdick used the augmented-plane-wave (APW) method and a potential due to Chodorow.[7] Burdick's values are in excellent agreement with those of Segall[8] who used the Green's-function method. In general our points agree fairly well with those of Burdick in both position and shape of band. There are, however, some discrepancies which occur at energy levels well below the Fermi level and which should not affect the shape of the Fermi surface. The d-like states, Γ_{12} at -0.58 and $\Gamma_{25'}$ at -0.64 Ry shift by approximately 0.1 Ry. Figure 3 shows this comparison for the Δ_1 representation ($\Gamma_{25'}$ is not shown in Fig. 3). The long-dashed curve of Fig. 3 is Cu obtained with our program by treating copper as though it were Cu_3Cu and using the Chodorow potential. Some 20 points were so calculated and the biggest difference between ours and Burdick's was 0.03 Ry (the high-symmetry points compare to within 0.002 Ry). The fact that the copper calculation is in good agreement with the accurate calculations of Segall and of Burdick when the same potential was used was taken as a satisfactory test of our method. It should be noted that our results are too high. This is to be expected since the variational-principle results converge from above and since we have not taken full advantage of periodicity when we use the unit cell of Cu_3Cu which contains four atoms. For Cu_3Cu we used the same value as Burdick for the lattice constant a. For Cu_3Au we used[9] the room-temperature value $a=7.0825$ a.u.

CONVERGENCE

In the following discussion k_{max} will denote the largest value of $|\mathbf{k}+\mathbf{K}|a/2\pi$ used for any particular representation. The high-symmetry points (Γ,R,X,M) were calculated using the MPW method. For these points the levels near the Fermi level are probably convergent to within 0.005 Ry. The k_{max} for these representations was ≥ 4 and a typical expansion used some 30 plane waves.

For the points of lower symmetry, we cannot get enough plane waves into the expansion using MPW without having extremely large matrices. This problem was resolved by first calculating these points roughly using the MPW method, estimating the Fermi level from this and then recalculating those points and representations having levels near the estimated Fermi level by using a modified form of the OPW method in which we orthogonalized the plane waves to the lower-lying (core) atomic orbitals only (for the gold atom we kept the $5s$, $5p$, $5d$, and $6s$ orbitals and for copper we kept the $3s$, $3p$, $3d$, and $4s$ orbitals). To be sure we were orthogonalizing to accurate solutions of the Schrödinger equation, we orthogonalized only to core states which were sufficiently tightly bound so as to have negligible

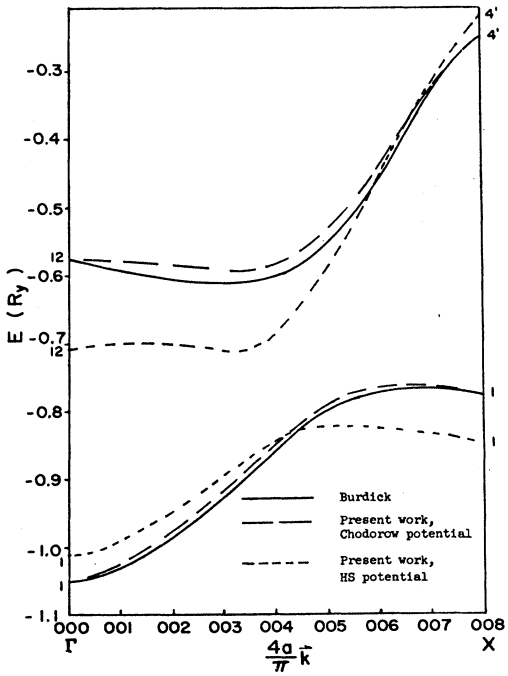

FIG. 3. Comparison of this calculation with Burdick's for the Δ_1 representation for Cu.

[5] We wish to thank Dr. R. A. Johnson for giving us the diagonalization program. This program was written by Dr. F. W. Quelle.

[6] G. A. Burdick, Phys. Rev. **129**, 138 (1963).

[7] M. I. Chodorow, Ph.D. thesis, Massachusetts Institute of Technology, 1939 (unpublished).

[8] B. Segall, Phys. Rev. **125**, 109 (1962).

[9] J. D. H. Donnay, G. Donnay, E. G. Cox, O. Kennard, and M. V. King, *Crystal Data Determinative Tables* (American Crystallographic Association, Washington, D. C., 1963), 2nd ed., p. 834.

overlap. The energy eigenvalues of these states in the crystal did not differ by more than 0.001 Ry from their free value. The points near the Fermi level calculated by OPW have been taken to a k_{max} of at least 3 and are probably convergent to within 0.01 Ry. Lower lying levels of low-symmetry points are probably convergent to between 0.01 and 0.02 Ry.

$E(k)$ CURVES AND DETERMINATION OF THE FERMI LEVEL

With the energy levels determined to the precision indicated above, curves of energy versus **k** were plotted in six principle directions in **k** space for energies in the range from −1.05 Ry to −0.1 Ry. These are shown in Figs. 4 through 9. (In the range from −0.8 to −0.6 Ry only the Δ_1, Σ_1 etc., representations are shown due to the large number of bands in this region.)

Coordinates for all **k** used along with the number of equivalent points for each are given in Table I. Table II lists $E(\mathbf{k})$ for 28 bands for all **k** considered. The points done by interpolation are listed for bands 21 through 24 only and are in parenthesis (these are the four bands near the Fermi level). Some of the very low symmetry points were also calculated by the computer as a check and the biggest discrepancy was 0.03 Ry. For those points both calculated and interpolated, Table II gives the lower of the two values. For the points with two elements in the group a plus sign (+) under the representation column refers to the representation in which both elements of the group have +1 matrices and a minus sign (−) refers to the representation in which

TABLE I. Values of **k** and the number of equivalent points for each **k**.

BSW[a] label	Order of group of **k**	Number of like vectors	Wave vector $4a\mathbf{k}/\pi$
Γ	48	1	000
Δ	8	6	001
Δ	8	6	002
Δ	8	6	003
X	16	3	004
Σ	4	12	110
Σ	4	12	220
Σ	4	12	330
M	16	3	440
Λ	6	8	111
Λ	6	8	222
Λ	6	8	333
R	48	1	444
Z	4	12	401
Z	4	12	402
Z	4	12	403
T	8	6	441
T	8	6	442
T	8	6	443
S	4	12	114
S	4	12	224
S	4	12	334
	2	24	102
	2	24	103
	2	24	203
	2	24	112
	2	24	113
	2	24	221
	2	24	223
	2	24	331
	2	24	332
	2	24	214
	2	24	314
	2	24	324
	1	48	123

[a] There are no BSW labels for the last 13 points.

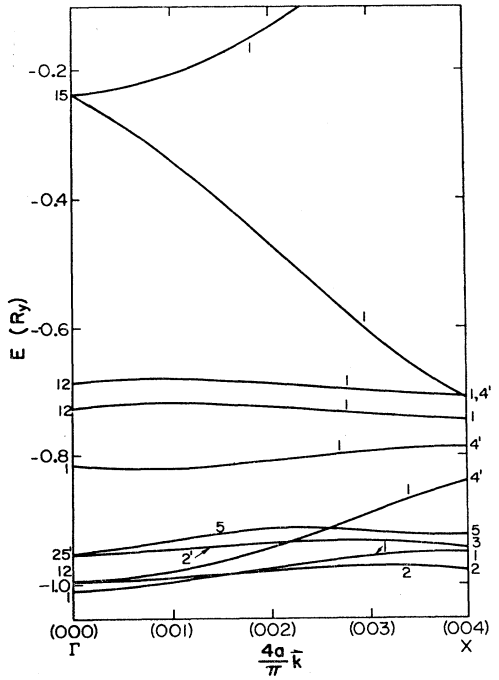

FIG. 4. E versus **k** for the $\Gamma\Delta X$ direction.

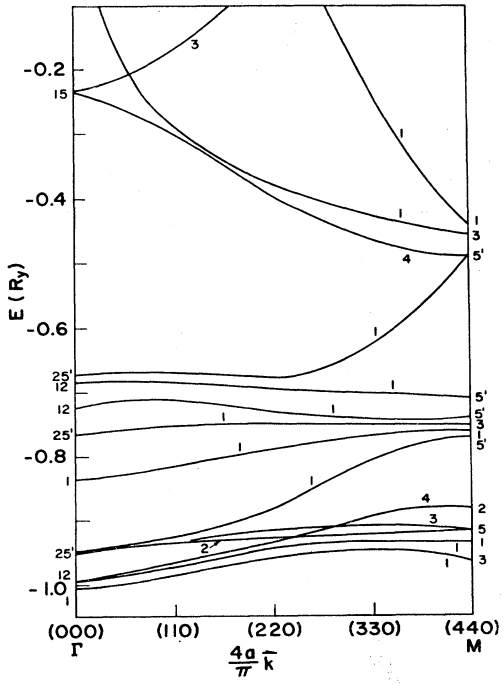

FIG. 5. E versus **k** for the $\Gamma\Sigma M$ direction.

TABLE II. E versus $\mathbf{k}$. The third and alternate columns give the representation in the BSW notation. The fourth and alternate columns give the energy eigenvalues for the respective bands.

BSW Label	$4a\mathbf{k}/\pi$	Rep.	Band 1	Rep.	Band 2	Rep.	Band 3	Rep.	Band 4
Γ	000	1	−1.004	12	−0.995	12	−0.995	25′	−0.951
R	444	25′	−0.972	25′	−0.972	25′	−0.972	12	−0.90
X	004	2	−0.970	1	−0.944	3	−0.94	5	−0.917
M	440	3	−0.964	1	−0.933	5	−0.916	5	−0.916
Δ	001	1	−0.993	2	−0.98	1	−0.974	2′	| 0.94
Δ	002	2	−0.974	1	−0.970	1	−0.944	2′	−0.932
Δ	003	2	−0.965	1	−0.948	2′	−0.927	5	−0.915
Σ	110	1	−0.981	1	−0.97	4	−0.968	2	−0.935
Σ	220	1	−0.956	1	−0.942	4	−0.937	2	−0.928
Σ	330	1	−0.951	1	−0.934	2	−0.918	3	−0.910
Λ	111	1	−0.969	3	−0.964	3	−0.964	3	−0.928
Λ	222	1	−0.94	3	−0.939	3	−0.939	3	−0.915
Λ	333	1	−0.959	3	−0.954	3	−0.954	3	−0.892
T	441	2′	−0.963	1	−0.921	5	−0.921	5	−0.921
T	442	2′	−0.967	5	−0.943	5	−0.943	1	−0.906
T	443	2′	−0.970	5	−0.966	5	−0.966	1	−0.895
S	114	4	−0.943	1	−0.930	3	−0.922	2	−0.919
S	224	3	−0.943	2	−0.939	1	−0.936	4	−0.917
S	334	3	−0.964	2	−0.959	1	−0.958	4	−0.897
Z	401	1	−0.948	1	−0.927	3	−0.921	4	−0.920
Z	402	1	−0.938	3	−0.938	4	−0.916	1	−0.903
Z	403	3	−0.954	1	−0.932	4	−0.913	2	−0.888
			Band 5		Band 6		Band 7		Band 8
Γ	000	25′	−0.951	25′	−0.951	1	−0.833	25′	−0.768
R	444	12	−0.90	1	−0.818	25′	−0.765	25′	−0.765
X	004	5	−0.917	4′	−0.839	4′	−0.791	2′	−0.780
M	440	2	−0.89	5′	−0.773	5′	−0.773	1	−0.765
Δ	001	5	−0.931	5	−0.931	1	−0.822	2′	−0.764
Δ	002	5	−0.923	5	−0.923	1	−0.813	2′	−0.770
Δ	003	5	−0.915	1	−0.882	1	−0.797	2′	−0.775
Σ	110	1	−0.93	3	−0.928	1	−0.82	3	−0.763
Σ	220	3	−0.917	1	−0.886	1	−0.797	3	−0.769
Σ	330	4	−0.894	1	−0.800	1	−0.771	3	−0.764
Λ	111	3	−0.928	1	−0.92	1	−0.81	1	−0.76
Λ	222	3	−0.915	1	−0.832	1	−0.78	1	−0.77
Λ	333	3	−0.892	1	−0.803	1	−0.773	3	−0.752
T	441	2	−0.875	1	−0.78	2′	−0.763	5	−0.763
T	442	2	−0.881	1	−0.797	2′	−0.765	5	−0.758
T	443	2	−0.887	1	−0.813	2′	−0.764	5	−0.762
S	114	1	−0.914	3	−0.813	3	−0.78	3	−0.77
S	224	1	−0.890	1	−0.786	3	−0.781	3	−0.754
S	334	1	−0.887	1	−0.807	3	−0.768	1	−0.759
Z	401	2	−0.875	3	−0.825	3	−0.782	2	−0.772
Z	402	2	−0.881	3	−0.798	3	−0.770	2	−0.763
Z	403	1	−0.877	3	−0.775	1	−0.769	1	−0.761
			Band 9		Band 10		Band 11		Band 12
Γ	000	25′	−0.768	25′	−0.768	12	−0.724	12	−0.724
R	444	25′	−0.765	15′	−0.747	15′	−0.747	15′	−0.747
X	004	5′	−0.755	5′	−0.755	1	−0.741	5	−0.721
M	440	2′	−0.761	4′	−0.756	3	−0.751	5′	−0.746
Δ	001	5	−0.756	5	−0.756	2	−0.72	1	−0.714
Δ	002	5	−0.750	5	−0.750	1	−0.730	2	−0.711
Δ	003	5	−0.746	5	−0.746	1	−0.737	5	−0.719
Σ	110	2	−0.756	1	−0.754	4	−0.72	1	−0.71
Σ	220	1	−0.751	2	−0.746	1	−0.730	4	−0.730
Σ	330	1	−0.753	4	−0.753	1	−0.743	3	−0.74
Λ	111	3	−0.752	3	−0.752	3	−0.71	3	−0.71
Λ	222	3	−0.746	3	−0.746	1	−0.73	3	−0.722
Λ	333	3	−0.752	3	−0.743	3	−0.743	1	−0.714
T	441	5	−0.763	5	−0.735	5	−0.735	2′	−0.734
T	442	5	−0.758	5	−0.739	5	−0.739	1′	−0.74
T	443	5	−0.762	5	−0.745	5	−0.745	1′	−0.74
S	114	1	−0.764	1	−0.750	4	−0.744	3	−0.73
S	224	1	−0.753	3	−0.74	2	−0.738	4	−0.736
S	334	2	−0.753	3	−0.745	4	−0.745	2	−0.735
Z	401	1	−0.753	1	−0.745	3	−0.729	4	−0.715
Z	402	1	−0.763	1	−0.755	3	−0.742	1	−0.729
Z	403	2	−0.754	3	−0.754	3	−0.748	4	−0.742

TABLE II (*continued*)

BSW Label	$4a\mathbf{k}/\pi$	Rep.	Band 13	Rep.	Band 14	Rep.	Band 15	Rep.	Band 16
Γ	000	12	−0.684	12	−0.684	2	−0.680	25′	−0.673
R	444	12	−0.684	12	−0.684	25′	−0.675	25′	−0.675
X	004	5	−0.721	2	−0.707	5′	−0.707	5′	−0.707
M	440	5′	−0.746	4	−0.721	5′	−0.716	5′	−0.716
Δ	001	2	−0.678	1	−0.676	5	−0.67	5	−0.67
Δ	002	5	−0.70	5	−0.70	1	−0.690	2	−0.685
Δ	003	5	−0.719	2	−0.706	1	−0.699	2	−0.694
Σ	110	1	−0.68	3	−0.68	4	−0.68	4	−0.67
Σ	220	3	−0.72	4	−0.713	4	−0.694	1	−0.692
Σ	330	4	−0.740	2	−0.725	4	−0.708	1	−0.700
Λ	111	1	−0.69	3	−0.68	3	−0.68	3	−0.68
Λ	222	3	−0.722	3	−0.716	3	−0.716	3	−0.69
Λ	333	2	−0.704	3	−0.699	3	−0.699	3	−0.677
T	441	1	−0.730	1′	−0.724	5	−0.720	5	−0.720
T	442	2′	−0.708	1	−0.704	5	−0.700	5	−0.700
T	443	1	−0.684	2′	−0.763	5	−0.679	5	−0.679
S	114	2	−0.723	4	−0.717	1	−0.712	2	−0.698
S	224	3	−0.73	1	−0.721	4	−0.72	2	−0.714
S	334	3	−0.699	4	−0.694	1	−0.692	3	−0.682
Z	401	1	−0.710	2	−0.702	4	−0.698	1	−0.694
Z	402	1	−0.719	2	−0.707	1	−0.700	4	−0.700
Z	403	1	−0.733	2	−0.710	1	−0.706	3	−0.705
			Band 17		Band 18		Band 19		Band 20
Γ	000	25′	−0.673	25′	−0.673	15′	−0.663	15′	−0.663
R	444	25′	−0.675	15′	−0.671	15′	−0.671	15′	−0.671
X	004	3′	−0.703	4′	−0.697	1	−0.697	3′	−0.689
M	440	5	−0.713	5	−0.713	3′	−0.707	1′	−0.701
Δ	001	2	−0.672	2′	−0.663	1′	−0.66	5	−0.66
Δ	002	2	−0.678	5	−0.67	5	−0.67	2′	−0.663
Δ	003	5	−0.69	5	−0.69	2	−0.684	2′	−0.663
Σ	110	1	−0.67	2	−0.668	4	−0.66	3	−0.66
Σ	220	2	−0.683	1	−0.683	4	−0.679	3	−0.67
Σ	330	4	−0.698	3	−0.69	2	−0.693	2	−0.682
Λ	111	3	−0.68	2	−0.67	3	−0.66	3	−0.66
Λ	222	3	−0.69	2	−0.686	3	−0.67	3	−0.67
Λ	333	3	−0.677	3	−0.670	3	−0.670	2	−0.643
T	441	2	−0.697	5	−0.694	5	−0.694	1′	−0.690
T	442	2	−0.688	5	−0.679	5	−0.679	1′	−0.679
T	443	2	−0.679	5	−0.670	5	−0.670	1′	−0.669
S	114	4	−0.68	2	−0.68	1	−0.670	2	−0.66
S	224	1	−0.675	4	−0.67	2	−0.67	2	−0.665
S	334	1	−0.673	2	−0.67	4	−0.669	2	−0.66
Z	401	3	−0.685	3	−0.685	3	−0.667	1	−0.664
Z	402	3	−0.693	3	−0.689	4	−0.658	2	−0.657
Z	403	4	−0.701	3	−0.697	2	−0.661	4	−0.659
			Band 21		Band 22		Band 23		Band 24
Γ	000	15′	−0.663	15	−0.236	15	−0.236	15	−0.236
R	444	2′	−0.455	15	−0.408	15	−0.408	15	−0.408
X	004	3	−0.670	1′	−0.665	5′	+0.08	5′	+0.08
M	440	5′	−0.492	5′	−0.492	3	−0.456	1	−0.440
Δ	001	5	−0.66	1	−0.321	5	−0.20	5	−0.20
Δ	002	1′	−0.66	1	−0.470	5	−0.13	5	−0.13
Δ	003	1′	−0.66	1	−0.604	5	−0.03	5	−0.03
Σ	110	2	−0.658	4	−0.294	1	−0.291	3	−0.18
Σ	220	2	−0.672	4	−0.397	1	−0.377	3	−0.05
Σ	330	1	−0.629	4	−0.466	1	−0.428	1	−0.235
Λ	111	2	−0.639	3	−0.268	3	−0.268	1	−0.27
Λ	222	2	−0.642	3	−0.324	3	−0.324	1	−0.32
Λ	333	1	−0.593	1	−0.393	3	−0.375	3	−0.375
T	441	5	−0.482	5	−0.482	2′	−0.454	1	−0.433
T	442	5	−0.462	5	−0.462	2′	−0.454	1	−0.424
T	443	2′	−0.454	5	−0.429	5	−0.429	1	−0.416
S	114	3	−0.658	1	−0.653	3	−0.08	4	−0.04
S	224	3	−0.596	1	−0.590	3	−0.25	4	−0.21
S	334	3	−0.507	1	−0.494	3	−0.376	4	−0.348
Z	401	4	−0.660	2	−0.654	3	−0.063	1	−0.034
Z	402	3	−0.622	1	−0.617	3	−0.220	1	−0.197
Z	403	3	−0.560	1	−0.555	3	−0.355	1	−0.341
	102	+	(−0.68)	+	−0.44	+	(−0.25)	−	−0.11

TABLE II (*continued*)

BSW Label	$4a\mathbf{k}/\pi$	Rep.	Band 21	Rep.	Band 22	Rep.	Band 23	Rep.	Band 24
	103	−	(−0.67)	+	−0.57	+	(−0.16)	−	−0.01
	203	+	−0.66	+	−0.52	+	−0.30	+	−0.09
	112	−	(−0.65)	+	(−0.40)	+	(−0.23)	−	(−0.23)
	223	+	(−0.63)	+	(−0.45)	+	(−0.29)	−	(−0.27)
	113	+	(−0.66)	+	(−0.53)	+	(−0.15)	−	(−0.10)
	221	−	(−0.66)	−	(−0.36)	+	(−0.35)	+	(−0.14)
	332	+	(−0.56)	−	(−0.39)	+	(−0.39)	+	(−0.37)
	331	+	(−0.60)	−	(−0.43)	+	(−0.41)	+	(−0.30)
	214	−	−0.61	+	−0.61	−	(−0.23)	+	(−0.21)
	314	−	−0.56	+	−0.55	−	(−0.35)	+	−0.33
	324	−	−0.54	+	−0.53	−	(−0.35)	+	−0.32
	123		(−0.64)		(−0.48)		(−0.29)		(−0.18)
			Band 25		Band 26		Band 27		Band 28
Γ	000	1	0.117	12	0.121	12	0.121	15	0.618
R	444	25′	−0.134	25′	−0.134	25′	−0.134	1	−0.071
X	004	5	0.082	5	0.082	3′	0.150	4′	0.154
M	440	2′	0.241	5′	0.322	5′	0.322	3	0.361
Δ	001	1	0.124	2	0.128	1	0.233	5	0.450
Δ	002	1	0.130	2	0.135	5	0.347	5	0.347
Δ	003	2	0.145	1	0.149	5	0.216	5	0.216
Σ	110	1	0.133	4	0.237	1	0.242	1	0.342
Σ	220	1	0.037	1	0.158	4	0.398	2	0.401
Σ	330	3	0.13	1	0.225	4	0.344	3	0.349
Λ	111	3	0.246	3	0.246	1	0.256	3	0.343
Λ	222	3	0.107	3	0.107	1	0.128	3	0.496
Λ	333	3	−0.068	3	−0.068	1	−0.047	1	0.139
T	441	2′	0.123	5	0.180	5	0.180	1	0.267
T	442	2′	−0.008	5	0.032	5	0.032	1	0.102
T	443	2′	−0.099	5	−0.088	5	−0.088	1	−0.028
S	114	2	−0.018	1	0.010	2	0.323	3	0.358
S	224	2	−0.090	1	−0.062	3	0.245	1	0.319
S	334	2	−0.123	1	−0.100	3	−0.007	1	0.048
Z	401	4	0.119	2	0.134	3	0.180	1	0.306
Z	402	2	0.166	3	0.178	4	0.179	1	0.315
Z	403	2	0.213	3	0.261	4	0.270	1	0.320

the nonidentity matrix is −1. The less precisely determined points are given to two significant figures only. No particular effort has been made to determine the precision of the higher levels (bands 25 through 28) as these are of secondary interest in this calculation.

We are now in a position to compute the Fermi level. Only the valence electrons contribute to the range of interest (−1.0 to 0.0 Ry). The other (core) electrons lie below this range and their $E(\mathbf{k})$ curves are essentially flat for all values of $\mathbf{k}$. It is thus necessary to account for 44 electrons from each unit cell (ten *d* electrons and one *s* electron from each of the four atoms). The allowed number of $\mathbf{k}$ values equals the total number of unit cells in the crystal considered so that in using 512 values of $\mathbf{k}$ we have $44\times512=22\,528$ electrons. As each $E_n(\mathbf{k})$ can hold two electrons (due to spin) the first 11 264 energy levels are occupied (at 0°K) and all levels above this are empty. By simply counting up the levels we obtain a Fermi level of −0.39 Ry. In counting these levels the first 21 bands can be counted *en masse* as 512 levels each. In counting the remaining 512 levels we must count each Δ listed in Table II as 6 levels; each Λ as 8 levels; etc.

CONSTRUCTION OF THE FERMI SURFACE AND COMPARISON WITH OTHER CALCULATIONS

In the following discussion we refer to our 21st, 22nd, 23rd, and 24th bands as the first, second, third, and fourth bands, respectively. As the first 20 bands are completely filled, this is in keeping with standard terminology. Knowing the Fermi level, we construct a Fermi surface by determining where the $E(\mathbf{k})$ curve for each $\mathbf{k}$ direction intersects the Fermi energy. Figure 10 shows the resulting Fermi surface as well as two sets of surfaces constructed by Harrison[10] based on folding from Cu to Cu_3Cu. Harrison constructed the upper set of Fig. 10 by starting with an (unfolded) spherical Fermi surface and the second set by starting with the Pippard model for copper. For our Fermi surface, cross sections in the (110) plane for zones 2, 3, and 4 are shown in Figs. 11, 12, and 13. It is noted that with our Fermi level of −0.39 Ry all four bands agree closely with the surface based on the Pippard model. We also note that in Harrison's constructions the first band is completely filled in the Pippard model, whereas there is

[10] W. Harrison, in W. Harrison and M. B. Webb, *The Fermi Surface* (John Wiley & Sons, Inc., New York, 1960), p. 28.

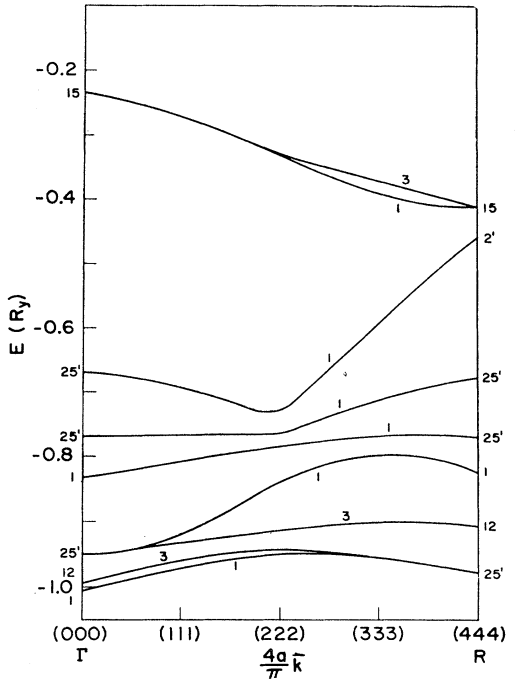

FIG. 6. E versus $\mathbf{k}$ for the $\Gamma\Lambda R$ direction.

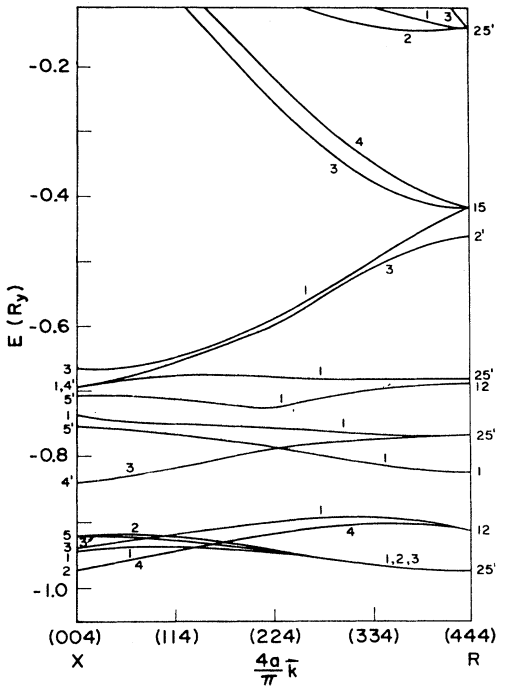

FIG. 8. E versus $\mathbf{k}$ for the XSR direction.

a small unfilled section around L (or R) in the free-electron model. It would be interesting to distinguish between these two cases experimentally. As it would require a drop of about 0.06 Ry from the -0.39 Ry value calculated by us to leave any unfilled section around R in the first band (see either Fig. 6, 7, or 8) it is felt that our calculation is consistent with the Pippard model in this regard.

The upper bands of Figs. 4 through 9 are consistent with what would be expected in a folding of Cu to

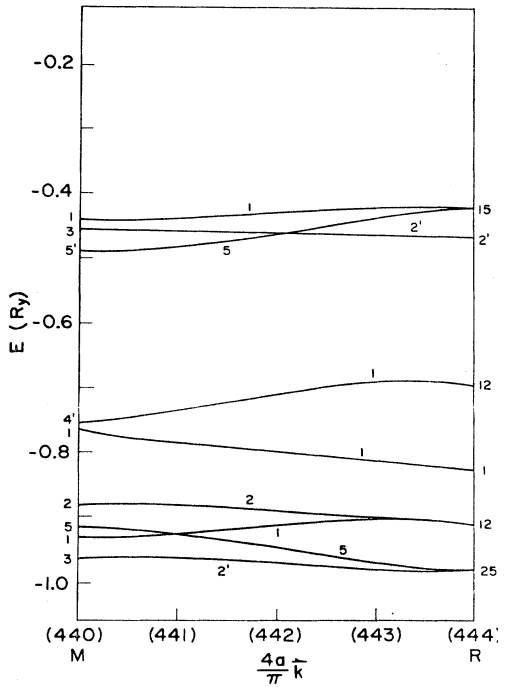

FIG. 7. E versus $\mathbf{k}$ for the MTR direction.

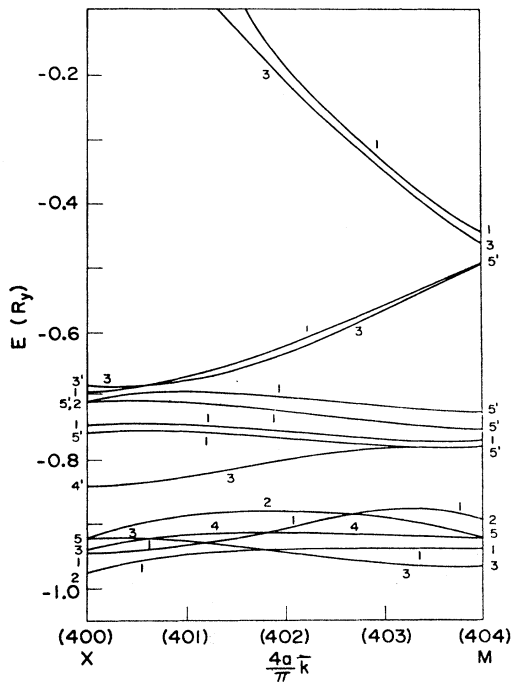

FIG. 9. E versus $\mathbf{k}$ for the XZM direction.

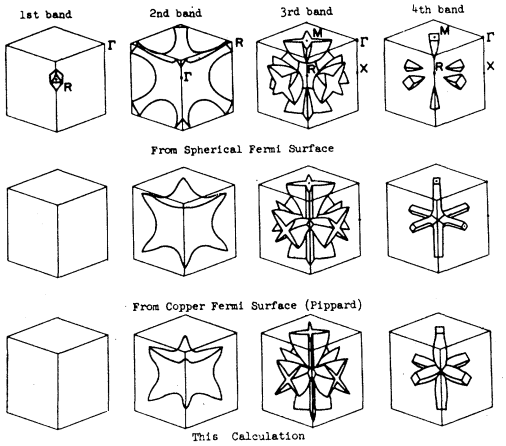

FIG. 10. Comparison of the calculated Cu_3Au Fermi surface with Harrison's folded surfaces.

Cu_3Cu. We use Fig. 5 to illustrate this. We emphasize that we are here concerned only with the change in Brillouin zone in going from the fcc lattice of Cu to the simple-cubic lattice of Cu_3Cu and not with an actual calculation of Cu or Cu_3Cu as such. The point M of Fig. 5 has 4 equivalent points in the simple-cubic reciprocal-space unit cell. For Cu, with a truncated octahedron reciprocal-space unit cell this M point is a Σ or interior point and has no other equivalent points. There would thus be four degenerate levels somewhere near -0.45 Ry for Cu_3Cu. The change from Cu_3Cu to Cu_3Au splits this degeneracy into the levels M_1 at -0.440, M_3 at -0.456 and $M_{5'}$ at -0.492. As $M_{5'}$ is two-dimensional, the degeneracy is not completely removed.

We now compare the band gaps of the present Fermi surface with those calculated by Giaever[11] using the nearly-free-electron model and the Hartree screening function. Giaever calculated the band gaps in the (100) and (110) planes from one adjustable parameter fit by three independent types of experiments (dilute alloy resistivity,[12] variation of Hall effect with ordering,[13] and the ratio of temperature coefficient of resistivity of ordered and disordered[14] Cu_3Au). With the assumption of an isotropic relaxation time all three ways gave band gaps of ≈ 0.03 and ≈ 0.04 Ry for the (100) and (110) planes, respectively. (Giaever gives normalized gaps $\Delta E_{100}/E_F \approx 0.06$ and $\Delta E_{110}/E_F \approx 0.08$. Using $E_F = 0.48$ based on a free-electron calculation gives the ΔE as stated above.) In our calculation we find no single value for the band gap in either plane but rather a range of values. This is to be expected when the fairly complicated nature of the band structure is considered. In the (100) face the gap (from third to fourth zone) ranges from ≈ 0.01 up to 0.03 and then down to ≈ 0.015 Ry as one goes from the Z direction to the S direction. As one goes along the XSR line from k_{Fermi} toward X, the gap opens up to a fairly constant value of 0.03 and then narrows to 0.005 Ry at X. The same is true for the

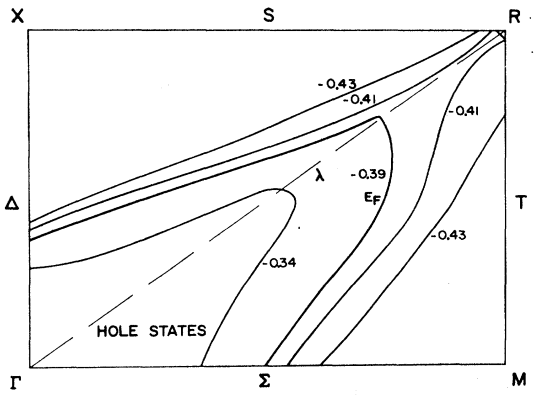

FIG. 11. Energy contours near the Fermi level in the (110) plane for the second zone.

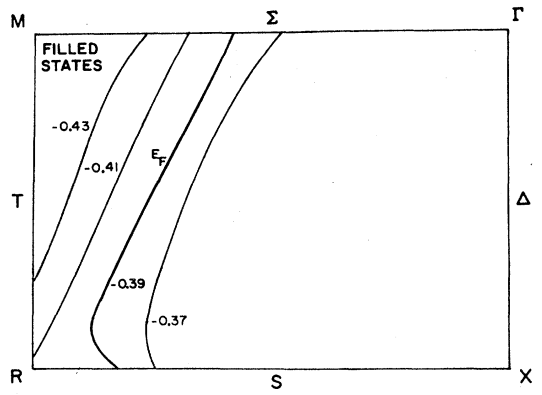

FIG. 12. Energy contours near the Fermi level in the (110) plane for the third zone.

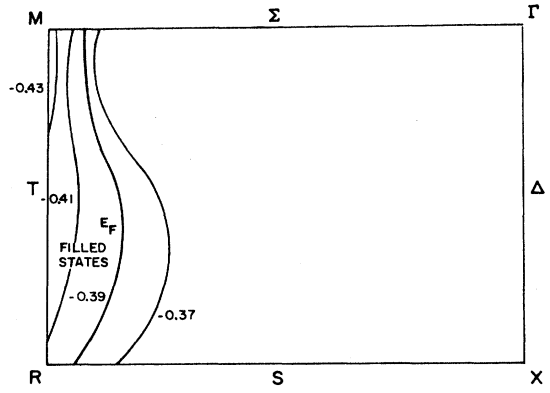

FIG. 13. Energy contours near the Fermi level in the (110) plane for the fourth zone.

[11] I. Giaever, Ph.D. thesis, Rensselaer Polytechnic Institute, 1964 (unpublished).

[12] F. Blatt, *Solid State Phys.* **4**, 199 (1956), in particular, p. 318.

[13] A. R. Von Neida and R. B. Gordon, Phil. Mag. **79**, 1129 (1962).

[14] M. C. Anquetil, J. Phys. Radium **23**, 113 (1962).

XZM direction with a fairly constant value of ≈ 0.025 Ry. In the (110) face the gap (from second to third zone) ranges from 0.02 to 0.002 as one goes from the Σ toward the Λ direction. Along the $\Gamma\Sigma M$ line the gap changes considerably as can be seen from Fig. 5. The band gaps in the present paper are thus seen to be of the same order of magnitude as those calculated by Giaever but differ both qualitatively and quantitatively.

To the best of our knowledge, standard Fermi-surface experiments such as the de Haas–van Alphen effect, magnetoresistance, magnetoacoustic effect, and cyclotron resonance have not yet been done for Cu_3Au. These experiments require a long mean free path and large samples of Cu_3Au with perfect (or nearly perfect) ordering are relatively difficult to obtain. Perhaps other types of experiments such as optical effects[15] and the polar Faraday effect[16] which do not require long mean free paths will be useful in determining the shape of the Cu_3Au Fermi surface.

CONCLUSIONS

It is felt that the computed Fermi level is accurate to between 0.02 and 0.03 Ry for the potential chosen. We note that the MPW method (in conjunction with OPW) converges without an exorbitant number of plane waves in the trial expansion functions. The surface calculated here agrees very well with Harrison's[10] construction based on the Pippard copper model. It appears that the nearly-free-electron approach, although adequate for a rough description, does not give a detailed picture of the Fermi surface of Cu_3Au.

We have seen some difference in $E(\mathbf{k})$ on going from the Herman-Skillman to the Chodorow potential but from the points sampled we feel that the shape of the Fermi surface should not be appreciably altered. Further experimental work on Cu_3Au is needed before a detailed comparison can be made between our calculated results and experiment.

ACKNOWLEDGMENTS

We wish to thank Peter Kapo, Dr. Frank Butler, and Dr. F. Kenneth Bloom for their help in running and debugging programs. We are also indebted to Dr. Bloom and Dr. Alma Marcus for many valuable discussions of the problem. A large amount of the computer work at New York University was done by mail and we are grateful to Henry Mullish for handling the running of programs there.

APPENDIX

The three types of $\mathbf{S}$ and $\mathbf{H}$ matrix elements are as listed below.

Plane-Wave–Plane-Wave

$$S_{\mathrm{pwpw}}=(\mathrm{Vol}/4\pi)\sum_R D_{11}(\mathbf{R})\delta[\mathbf{k}+\mathbf{K}',\mathbf{R}(\mathbf{k}+\mathbf{K})],$$

where

$$\mathrm{Vol}=\text{volume of the unit cell},$$

$$\delta(x,y)=0,\quad x\neq y$$
$$=1,\quad x=y$$

$$H_{\mathrm{pwpw}}=[(\mathbf{k}+\mathbf{K})^2+\bar{V}]S_{\mathrm{pwpw}}$$
$$+\sum_R D_{11}(\mathbf{R})\left[\int_0^{R_s}(rV_{\mathrm{Au}}(r)-r\bar{V})j_0(|\mathbf{K}_1|r)rdr\right.$$
$$\left.+\sum_{\mathrm{Cu}}\exp(i\mathbf{K}_1\cdot\mathbf{s}_\nu)\int_0^{R_s}(rV_{\mathrm{Cu}}(r)-r\bar{V})j_0(|\mathbf{K}_1|r)rdr\right],$$

where $\mathbf{K}_1=\mathbf{R}(\mathbf{k}+\mathbf{K})-(\mathbf{k}+\mathbf{K}')$ and R_s is the radius of the appropriate muffin-tin sphere.

Atomic-Term–Plane-Wave

$$S_{\mathrm{atpw}}=\int_0^{R_s}U_{nl}(r)j_l(|\mathbf{k}+\mathbf{K}|r)rdr$$
$$\times\sum_R D_{11}(\mathbf{R})X_{lj}(\mathbf{B})\exp(i\mathbf{K}_2\cdot\mathbf{s}_\nu),$$

$$H_{\mathrm{atpw}}=(\mathbf{k}+\mathbf{K})^2S_{\mathrm{atpw}}$$
$$+\int_0^{R_s}U_{nl}(r)j_l(|\mathbf{k}+\mathbf{K}|r)V_\nu(r)rdr$$
$$\times\sum_R D_{11}(\mathbf{R})X_{lj}(\mathbf{B})\exp(i\mathbf{K}_2\cdot\mathbf{s}_\nu),$$

where $\mathbf{K}_2=\mathbf{R}(\mathbf{k}+\mathbf{K})-\mathbf{k}$ and $\mathbf{B}=\mathbf{R}(\mathbf{k}+\mathbf{K})/|\mathbf{k}+\mathbf{K}|$.

The atomic orbitals are expressed as

$$F_{nlm}(r)=i^l[U_{nl}(r)/r]X_{lj}(\mathbf{r}/r),$$

where

$$X_{lj}(\mathbf{r}/r)=\sum_m a(lj;m)Y_{lm}(\mathbf{r}/r)$$

and the Y_{lm} are spherical harmonics. The i^l was added to make the $\mathbf{S}$ matrix real.

Atomic-Term–Atomic-Term

$$S_{\mathrm{atat}}=(1/4\pi)\int_0^{R_s}U_{nl}(r)U_{n'l}(r)dr$$
$$\times\sum_R{}' D_{11}(\mathbf{R})\exp[i\mathbf{k}\cdot(\mathbf{R}\mathbf{s}_\nu-\mathbf{s}_\nu)]$$
$$\times\int X_{lj}\left(\frac{\mathbf{r}}{r}\right)X_{lj'}\left(\frac{\mathbf{R}\mathbf{r}}{r}\right)d\Omega.$$

$$H_{\mathrm{atat}}=\frac{1}{4\pi}\sum_R{}' D_{11}(\mathbf{R})\exp[i\mathbf{k}\cdot(\mathbf{R}\mathbf{s}_\nu-\mathbf{s}_\nu)]$$
$$\times\int F^*_{nlm}(\mathbf{R}\mathbf{r})[-\nabla^2+V_\nu(r)]F_{n'lm'}(r)d\tau.$$

The prime on the $\mathbf{R}$ sum indicates that only those $\mathbf{R}$ for which some $\boldsymbol{\tau}$ satisfies $\mathbf{R}\mathbf{s}_\nu=\boldsymbol{\tau}+\mathbf{s}_{\nu'}$ are allowed. In the equations in this Appendix, $\mathbf{K}$ and $\mathbf{K}'$ are reciprocal lattice vectors and j_l is the lth spherical Bessel function. The subscript ν runs over the one gold and three copper basis atoms.

[15] M. Suffczynski, Phys. Status Solidi 4, 3 (1964).
[16] J. C. McGroddy *et al.*, Phys. Rev. **139**, A1844 (1965).